

In Vitro Cytocompatibility and Osteogenic Potential of Biodegradable Mg–Sr Alloys



Chen Liu, Lili Tan, Ying Zhao, Peng Wan, Haobo Pan, Xinbing Zhao, Yongdong Xu and Ke Yang

Abstract The cytocompatibility and osteogenic ability of novel as-extruded Mg–xSr ($x = 0.25, 1.0, 1.5, 2.5$ wt%) alloys are systematically investigated by in vitro cell adhesion and proliferation, alkaline phosphatase (ALP) activity, real-time RT-PCR evaluation, and mineralization tests. The results indicate that in addition to no cytotoxicity towards MC3T3-E1 cells, the Mg–Sr alloys, particularly Mg–1.5Sr, obviously promote the adhesion, proliferation, alkaline phosphatase activity, matrix mineralization and collagen secretion of MC3T3-E1 cells compared to pure Mg. Nearly all the osteogenesis-related genes, namely Runx2, Opn, Sp7, and Bmp2, are up-regulated for Mg–xSr, compared to pure Mg. In particular, Mg–1.5Sr reveals the best osteogenic ability. Our work suggest that novel as-extruded Mg–1.5Sr alloy, which exhibits excellent in vitro cytocompatibility and osteogenic ability, is promising in expediting clinical acceptance of biodegradable magnesium alloys.

Keywords Magnesium alloys · Cytocompatibility · Osteogenesis Strontium

C Liu and L. Tan these two authors contributed equally to this paper.

C. Liu · X. Zhao
Department of Materials Science and Engineering,
Zhejiang University, Hangzhou, China
e-mail: chenliu52s@163.com

C. Liu · Y. Xu
Ningbo Branch of Chinese Academy of Ordnance Science, Ningbo, China

L. Tan · P. Wan · K. Yang (✉)
Institute of Metal Research, Chinese Academy of Sciences, Shenyang, China
e-mail: kyang@imr.ac.cn

L. Tan
e-mail: lltan@imr.ac.cn

Y. Zhao (✉) · H. Pan
Shenzhen Institutes of Advanced Technology,
Chinese Academy of Sciences, Shenzhen, China
e-mail: ying.zhao@siat.ac.cn

Introduction

Due to the specific physical properties and chemical structure, magnesium-based metals possess significant advantages compared with the traditional metallic implant materials [1–5]. They have been demonstrated with extraordinary biological properties, including (1) excellent biocompatibility: magnesium is an indispensable element in the body. Mg^{2+} is involved in many metabolic reactions; (2) unique degradability: magnesium and its alloys can easily corrode in physiological environment so that repeated surgery for implant removal is not needed; (3) appropriate mechanical properties: the elastic moduli of magnesium alloys are similar to those of cortical bones, which can effectively avoid the stress shielding effect. Based on above advantages, Mg-based metals have been widely studied in recent years as potentially biodegradable metallic materials for implantation applications, especially in orthopedic fields [6–8].

An ideal magnesium alloy implant would maintain mechanical integrity in the human body for at least 12 weeks. While the bone tissue heals, it will eventually be replaced by new bone tissue [9, 10]. It is also important that the corrosion rate and degradation products, such as subcutaneous gas bubbles, should be within the body's acceptable ranges [11]. However, magnesium is highly liable to corrode in physiological conditions that contains chloride ion, which accordingly results in a dramatically decrease in its mechanical properties prior to the tissue healing [12–14]. From the material perspective, alloying may be an effective approach to diminish the degradation rates of magnesium alloys. Alloying elements such as aluminum, manganese, zinc, calcium, and rare earth metals have been used to improve the mechanical properties and reduce the corrosion rate of Mg [15–18]. However, from the perspective of *in vivo* application, not all the alloying elements are suitable. Aluminum is well known as a neurotoxicant and its accumulation has been suggested to be an associated phenomenon in various neurological disorders [19]. Severe hepatotoxicity has been detected after the administration of those rare earth metals of cerium, praseodymium and yttrium [20]. Comparatively, calcium, manganese, zinc and perhaps a very small amount of low toxicity rare earth elements are optional as suitable alloying elements for biodegradable Mg alloys.

Strontium (Sr) has been recently reported as a potential alloying element for medical applications [13]. From the standpoint of corrosion and mechanical properties, Sr can improve the mechanical properties and corrosion resistance of certain Mg alloys. Zeng et al. reported that Sr had a significant grain-refinement effect in AZ31 magnesium alloy and could improve both yield strength and elongation of AZ31 alloy [21]. Fan et al. indicated that Sr could improve both the mechanical properties and corrosion resistance of AZ91D magnesium alloy in NaCl solution due to the formation of Al_4Sr phase [22]. From the viewpoint of biocompatibility, Sr is a natural component in human bones and about 98% of Sr in human body is localized in bone tissues [12, 23]. The role of Sr in bone is known to promote the growth of osteoblasts and prevent bone resorption [24]. With aid of the bone formation stimulation effect by Sr, Sr salts at low dose were put forward as a

therapeutic agent to treat osteoporosis through increasing the bone mass and reducing the incidence of fractures [25, 26]. Sr-substituted hydroxyapatite (SrHA) was demonstrated to exert a positive effect on osteogenesis around the bone cement interface [27, 28].

Recently, novel as-rolled Mg–Sr alloys have been developed for skeletal applications. It is reported that as-rolled Mg–2Sr alloy possessed the best combination of corrosion resistance, high strength and in vivo biocompatibility among various Mg–Sr alloys (with Sr contents ranging from 1 to 4 wt%) [13]. Brar et al. studied as-cast Mg–xSr ($x = 0.5, 1.0, 1.5$ wt%) alloys and found the lowest degradation rate from Mg–0.5Sr [29]. Bornapour et al. indicated that the as-cast Mg–0.5Sr with a slow degradation rate could not lead to thrombosis during three weeks of implantation and a Sr-substituted HA layer was formed on Mg–0.5Sr which is known to enhance bone cell growth and proliferation around bone implants [12]. Additionally, our previous work has confirmed that the as-extruded Mg–xSr ($x = 0.25, 1.0, 1.5, 2.5$ wt%) alloys possessed similar mechanical properties to cortical bone, controlled corrosion rates, good cytocompatibility as well as excellent antibacterial properties [30]. The above results show that superior Mg–Sr alloys can be used as potential candidate for future orthopedic applications. However, up till now a comprehensive evaluation of osteogenic ability of as-extruded Mg–Sr alloy is not reported. The aim of this study was to examine the in vitro cytocompatibility and osteogenic ability of biodegradable Mg–Sr alloys.

Materials and Methods

Materials preparation. The experimental binary Mg–xSr ($x = 0.5, 1.5, 2.5, 4.0$ wt %) alloys were fabricated using pure Mg (99.9%) and a Mg-30wt% Sr master alloy in a high-purity graphite crucible under the protection of a mixed gas atmosphere of SF₆ (1 vol%) and carbon dioxide (CO₂). The melting was held at 730 °C for 30 min and stirred with a graphite rod. The melt was then poured into a steel mold pre-heated to 300 °C. The binary Mg–Sr alloys were encapsulated in quartz tubes under vacuum and then homogenization treated at 500 °C for 20 h followed by quenching in water. The as-cast ingots were hot extruded into bars at 390 °C with extrusion ratio of 64:1. The as-extruded pure Mg was prepared following the aforementioned procedure as the control group. It was subsequently machined into samples with dimensions of $\Phi 10 \times 3$ mm³. All the samples were ground with SiC papers up to 2000 grit, ultrasonically cleaned in acetone, absolute ethanol and distilled water in turn, and finally dried. The compositions of the Mg–Sr alloys measured by inductively coupled plasma atomic emission spectrometry (ICP-AES, Optima 7300DV, USA) are listed in Table 1.

Extracts preparation. Extracts were prepared using serum-free modified Eagle's medium alpha (α -MEM, Hyclone, USA) as the extraction medium with a ratio of extraction medium/sample surface area of about 1.25 cm²/mL in a humidified atmosphere containing 5% CO₂ at 37 °C for 24 h according to the ISO 10993-5.

Table 1 Chemical composition of the Mg–Sr alloys (wt%)

Nominal composition		Mg–0.5Sr	Mg–1.5Sr	Mg–2.5Sr	Mg–4.0Sr
Actual composition	Sr	0.25	1.0	1.5	2.5
	Mg	Balance			

Mg magnesium; *Sr* strontium

Prior to immersion, the samples were sterilized by ultraviolet irradiation for 30 min. After immersion, the supernatant was withdrawn, centrifuged, and filtered to prepare the extraction medium. It was remained at 4 °C prior to cell tests and the extract from pure Mg served as the control.

Cytotoxicity and cell proliferation assay. The cytotoxicity and cell proliferation were evaluated by an indirect contact assay according to ISO 10993-5. Murine calvarial preosteoblasts (MC3T3-E1, ATCC CRL-2594) were seeded on 96-well cell culture plates at an initial density of 5×10^3 cells/100 mL and incubated for 24 h to allow cell attachment. The medium was then replaced with 100 μ L of the extracts. After culturing for 1, 3, and 5 days, MTT solutions were added to each well and incubated at 37 °C for 4 h to form formazan which was then dissolved using dimethyl sulfoxide (DMSO). The optical density (OD) was determined on a microplate reader (Thermo Scientific Multiskan GO, USA) at 490 nm with a reference wavelength of 570 nm to determine the cell viability in comparison with the control.

Live/dead staining. The MC3T3-E1 cells were seeded on 12-well cell culture plates at a density of 2×10^4 cells/well for 24 h to allow cell attachment. The medium except the control group was then replaced by 500 μ L of the extracts. After incubation for another 24 h, the cells adhered to the plates and cultured in extracts were stained by the Live/Dead staining. The living and dead cells were, respectively, stained with Calcein-AM and iodide pyridine (Sigma) for 30 min at 37 °C, and then visualized using a fluorescence microscope (Olympus IX71, Japan).

Cell morphology. The MC3T3-E1 cells were seeded on 12-well cell culture plates at a density of 2×10^4 cells/well for 24 h to allow cell attachment. The medium except the control group was then replaced by 500 μ L of the extracts. After incubation for 12 h, the unattached cells were removed by rinsing with phosphate buffered saline (PBS) solution. The cells were fixed with 4% paraformaldehyde at 4 °C for 30 min and permeabilized with 0.5% Triton X-100 in PBS solution for 5 min. The cells were subsequently rinsed with PBS solution and the F-actin stress fibers and nuclei were stained with rhodamine phalloidin (Cytoskeleton, USA) and 40, 6-diamidino-2- phenylindole (DAPI, Dojindo, Japan), respectively. The cytoskeleton and cell nuclei were observed by fluorescence microscopy (Olympus IX71, Japan).

Alkaline phosphatase (ALP) activity. The MC3T3-E1 cells were seeded on 12-well cell culture plates at a density of 3×10^4 cells/well and incubated in different extracts supplemented with 100 nM dexamethasone, 0.2 mM ascorbic

acid, and 10 mM β -glycerophosphate. The extracts were changed every 3 days. After 4, 7 and 14 days, the cells were washed three times with PBS and lysed in 0.2 vol% Triton X-100. The alkaline phosphatase (ALP) activity was determined by a colorimetric assay using an ALP reagent containing p-nitrophenyl phosphate (p-NPP) as the substrate (Beyotime, China). The absorbance of p-nitrophenol was monitored at 405 nm. The intracellular total protein content was determined using the MicroBCA protein assay kit (Thermo Pierce, USA) and the ALP activity was normalized to the total protein content.

Extracellular matrix (ECM) mineralization and collagen secretion. The extracellular matrix (ECM) mineralization and collagen secretion by the MC3T3-E1 cells in the Mg–Sr alloys extracts were evaluated by the Alizarin Red and Sirius Red staining, respectively. After incubating for 15 days, the cells with an initial concentration of 3×10^4 /well were washed and fixed. Afterwards, they were stained using 40 mM Alizarin Red (Sigma) at a pH of 4.2 to show the mineralization or 0.1% Sirius Red (Sigma) to reveal the collagen. The unbound stain was washed with distilled water or 0.1 M acetic acid prior to photographing by a digital camera (Nikon D3200, Japan). In the quantitative analysis, the Alizarin Red or Sirius Red stain was dissolved in 10% cetylpyridinium chloride in 10 mM sodium phosphate (pH 7) or 0.2 M NaOH/methanol (1:1). The absorbance was measured at 620 or 540 nm.

Real-time polymerase reaction (RT-PCR). RT-PCR was used to assess the expression of the osteogenesis-related genes. The MC3T3-E1 cells were seeded on 12-well culture plates at a cell density of 3×10^4 cells/well and after 24 h, the culture medium was replaced by different material extracts supplemented with fresh serum. The MC3T3-E1 cells were incubated for 7, 10 and 14 days. The total RNA was isolated using a Trizol reagent (Invitrogen, USA) and the concentration of RNA was detected by measuring the optical absorbance at 260 nm on the Thermo 2000c (USA). 1 μ g of the RNA was reversely transcribed into complementary DNA (cDNA) using Superscript III (Invitrogen, USA) in a volume of 20 μ l. The forward and reverse primers of the selected genes are listed in Table 2. The expressions of the osteogenesis-related genes, including runt-related transcription factor 2 (Runx2), osteopontin (Opn), osterix (Sp7) and bone morphogenetic protein-2 (Bmp2) were quantified by Real-time PCR (Biorad

Table 2 Primer pairs used in real-time PCR analysis

Gene	Forward primer	Reverse primer
Mouse β -actin	5'-GGCTGTATTCCCCTCCATCG-3'	5'-CCAGTTGGTAACAATGCCATGT-3'
Runx2	5'-AGAGTCAGATTACAGATCCC AGG-3'	5'-TGGCTCTTCTACTGAGAGAGG - 3'
Opn	5'-TCTGATGAGACCGTCACTGC-3'	5'-AGGTCCTCATCTGTGGCATC-3'
Sp7	5'-ATGGCGTCTCTCTGCTTG-3'	5'-TGAAAGGTCAGCGTATGGCTT-3'
Bmp2	5'-GGGACCCGCTGTCTTCTAGT-3'	5'-TCAACTCAAATTCGCTGAGGAC-3'

CFX96, USA) on the SYBR Green PCR Master Mix (Applied Biosystems, USA). The relative mRNA expression level of each gene was normalized to the house-keeping gene β -actin (mouse β -actin) and determined by the Ct values.

Statistical analysis. The cell tests were performed in triplicate. The experimental results were expressed as mean \pm standard deviations and the data were analyzed using SPSS 13.0 software. A two-way analysis of variance (ANOVA) followed by a Student-Newman-Keuls post hoc test was used to determine the level of significance in cytotoxicity, cell proliferation, ALP activity and osteogenesis-related gene expressions assay, and an one-way ANOVA in extracellular matrix mineralization and collagen secretion test. $p < 0.05$ was considered to be statistically significant, and $p < 0.01$ was considered to be highly statistically significant.

Results and Discussions

Cytotoxicity. Figure 1 illustrates the relative cell growth rates of murine calvarial preosteoblasts MC3T3-E1 after 1, 3, and 5 days of incubation in the extracts of as-extruded Mg-xSr alloy ($x = 0.25, 1.0, 1.5, 2.5$ wt%) and pure Mg, respectively. It can be seen that no cytotoxicity is found for all the as-extruded Mg-Sr alloys and their cell viabilities are shown over 100% and higher than that of pure Mg, especially after 3 and 5 days culture ($\#p < 0.05$, $\#\#p < 0.01$). The extract of the as-extruded Mg-1.5Sr alloy leads to the highest cell viability. All Mg-Sr alloys reveal Grade 0 cytotoxicity according to ISO10993-5, suggesting good cytocompatibility and acceptable biosafety for in vivo applications.

Cell proliferation. Figure 2 shows MC3T3-E1 cells proliferation of as-extruded Mg-Sr alloys and pure Mg extraction mediums after 1, 3, and 5 days of incubation. It can be found that the cells number for all the as-extruded Mg-Sr alloy extracts

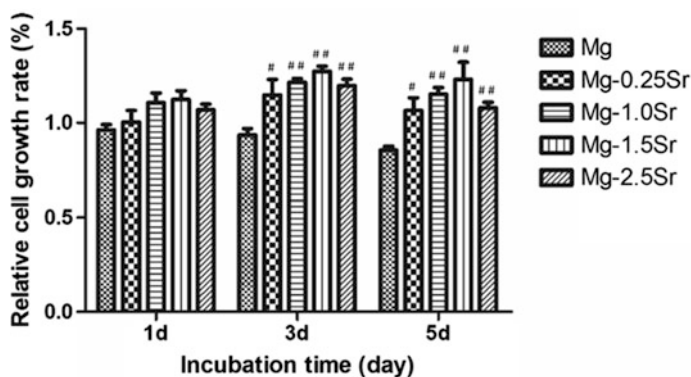
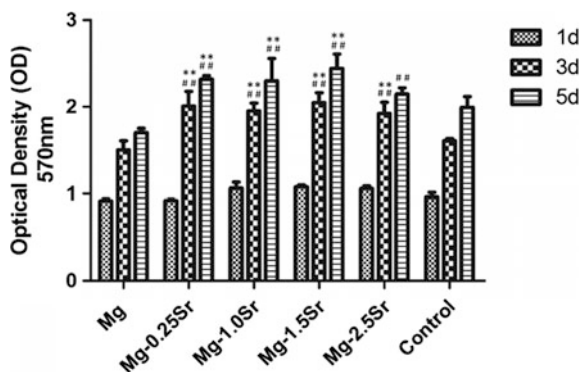


Fig. 1 Relative cell growth rates after 1, 3, and 5 days of incubation in the extracts of as-extruded Mg-Sr alloys and pure Mg. $\#p < 0.05$ and $\#\#p < 0.01$ compared with pure Mg

Fig. 2 Comparison of proliferation of MC3T3-E1 cells cultured in as-extruded Mg–Sr alloy and pure Mg extraction mediums for 1, 3, and 5 days. $**p < 0.01$ compared to the Control; $##p < 0.01$ compared to pure Mg



shows no significant difference when compared with pure Mg and control group on Day 1. However, after 3 days incubation, the cells number of as-extruded Mg–Sr alloys rise up dramatically and exceed pure Mg and control group, while pure Mg group shows slightly lower than the control group. After 5 days, the MC3T3-E1 cells incubated in all Mg–Sr alloys group show further increase. In particular, Mg–1.5Sr group rises significantly. These results indicate Mg–Sr alloys effectively promote MC3T3-E1 cells proliferation compared to pure Mg and control group, suggesting that Sr addition significantly improves in vitro cytocompatibility of magnesium metals.

Cell adhesion. Figure 3 depicts the Live/dead staining of MC3T3-E1 cells after 24 h of incubation in the extracts of as-extruded Mg–Sr alloys and pure Mg, respectively. Typical microscope fields are selected to show viable (green) and non-viable (red) cells. It is observed that most cells in all groups are stained green with occasionally distributed red-stained non-viable cells. The numbers of the viable cells in pure Mg and Mg–0.25Sr groups are similar to that of the control. With increasing Sr content in the alloys, more viable cells are observed, and the cells almost reach to 100% confluence in Mg–1.5Sr group. In comparison, the viable cells in the Mg–2.5Sr group are slightly decreased, but still higher than that of the control. The results indicate Mg–Sr alloy with appropriate Sr amount is favorable to enhance cytocompatibility of magnesium metals.

Cell morphology. Figure 4 reveals the cytoskeletons of the MC3T3-E1 cells after incubation for 12 h in extracts of as-extruded Mg–Sr alloys and pure Mg, respectively. Compared to the control, the attached cells for the pure Mg and as-extruded Mg–Sr alloys extracts show more spreading and superior filopodia extension. For the as-extruded Mg–Sr alloys, the cells are polygonal, elongated and thicker, with fine pseudopodia extension. The MC3T3-E1 cells cultured in the Mg–1.0Sr and Mg–1.5Sr extracts show more plump focal adhesion via well-organized F-actin stress fibers (red filaments) compared to Mg–0.25Sr and Mg–2.5Sr.

Osteogenic differentiation. Figure 5 shows the ALP activity of the MC3T3-E1 cells after incubation for 4, 7 and 14 days in extracts of as-extruded Mg–Sr alloys

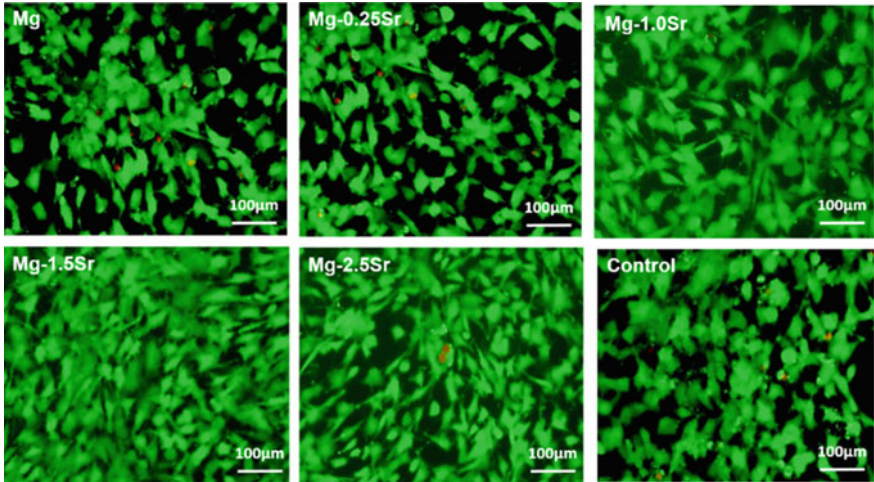


Fig. 3 Live/dead staining of MC3T3-E1 cells after 24 h of incubation in the extracts of as-extruded Mg–Sr alloys and pure Mg. Calcein-AM for viable cells (green) and iodide pyridine for non-viable cells (red)

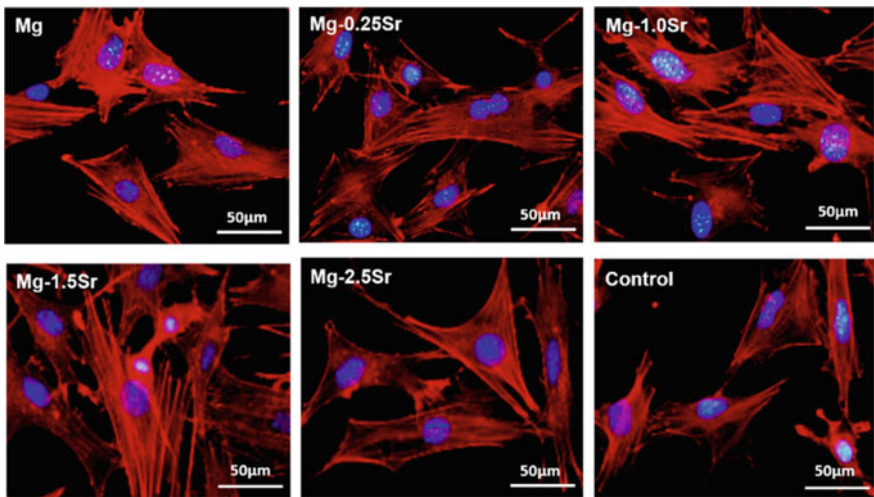


Fig. 4 Cytoskeleton staining of MC3T3-E1 cells after 12 h of incubation in the extracts of as-extruded Mg–Sr alloys and pure Mg. DAPI for nuclei (blue) and rhodamine phalloidin for F-actin stress fibers (red)

and pure Mg. There is no significant difference among all the extracts on day 4. After incubation for 7 days, ALP levels of the Mg–Sr alloys are significantly enhanced compared to those of pure Mg and control. The distinct ALP activities are emerged after 14 days incubation. Mg–1.5Sr shows the highest ALP activity which is

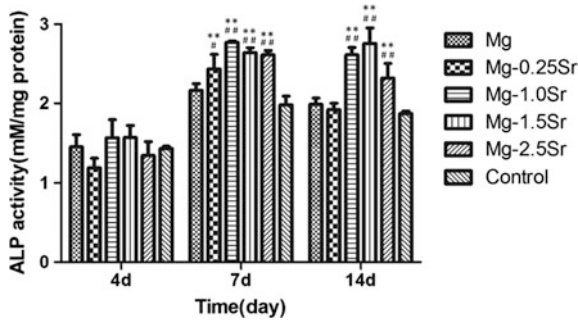


Fig. 5 ALP activity of MC3T3-E1 cells after incubation for 4, 7, and 14 days in the extracts of as-extruded Mg–Sr alloys and pure Mg. $**p < 0.01$ compared to the control; $\#p < 0.05$ and $\#\#p < 0.01$ compared to pure Mg

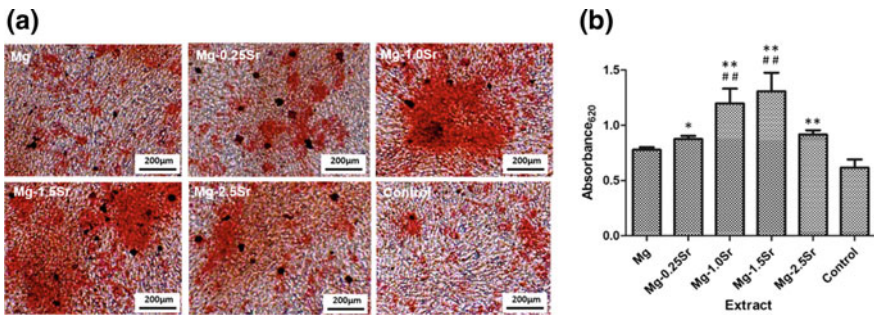


Fig. 6 **a** Extracellular matrix mineralization of MC3T3-E1 cells after incubation for 15 days in the extracts of as-extruded Mg–Sr alloys and pure Mg and **b** colorimetrically quantitative analysis. $*p < 0.05$ and $**p < 0.01$ compared to the control; $\#\#p < 0.01$ compared to pure Mg

followed by Mg–1.0Sr, Mg–2.5Sr, pure Mg and Mg–0.25Sr in sequence. The ALP activity of Mg–1.0Sr and Mg–1.5Sr are higher than those of pure Mg and control throughout the experimental period, showing the best osteogenic differentiation.

Figure 6 displays the ECM mineralization of MC3T3-E1 cells after incubation for 15 days in various Mg–Sr alloys and pure Mg extracts together with the corresponding quantitative colorimetric analysis. Figure 6a reveals mineralized calcium nodules formed in various extracts. A small portion of the stained calcium nodules in the pure Mg extract suggests a relatively weak extracellular calcium deposition. Comparatively, more depositions are observed in the Mg–Sr alloys extracts, especially for Mg–1.0Sr and Mg–1.5Sr. Correspondingly, the quantitative results as shown in Fig. 6b indicate that significant enhanced ECM mineralizations are detected in the Mg–1.0Sr and Mg–1.5Sr extracts compared to other groups. The ECM mineralization levels in Mg–0.25Sr and Mg–2.5Sr extracts are lower than those in Mg–1.0Sr and Mg–1.5Sr ones, but still higher than the pure Mg and control.

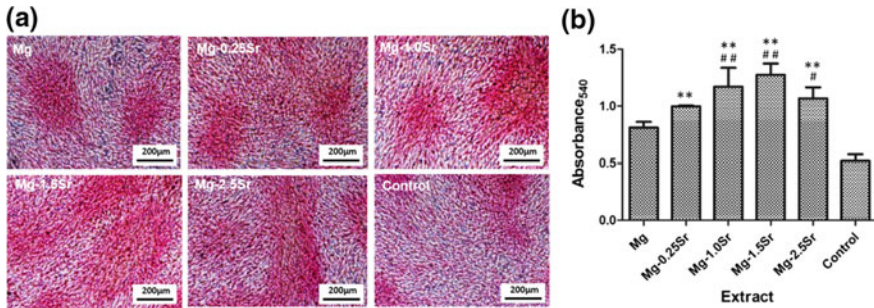


Fig. 7 **a** Collagen secretion from MC3T3-E1 cells after incubation for 15 days in the extracts of as-extruded Mg–Sr alloys and pure Mg and **b** colorimetrically quantitative analysis. ** $p < 0.01$ compared to the control; # $p < 0.05$ and ## $p < 0.01$ compared to pure Mg

Figure 7 depicts collagen secretion from MC3T3-E1 cells after incubation for 15 days in the extracts of as-extruded Mg–Sr alloys and pure Mg together with the corresponding quantitative colorimetric analysis. Figure 7a shows that denser collagens are secreted in the extracts of the Mg–Sr alloys than pure Mg and control. The collagen stained in the extract of pure Mg is less than those of Mg–Sr alloys and no significant clumps of collagen are deposited in control. According to the quantitative analysis in Fig. 7b, collagen secretion in the extracts of the Mg–Sr alloys are significantly promoted to about 123, 144, 157 and 132% compared to pure Mg, and 192, 225, 246 and 205% relative to the control, respectively.

Osteogenesis-related gene expressions. Figure 8 shows the osteogenesis-related gene expressions of Runx2, Opn, Sp7 and Bmp2 after culture for 7, 10, and 14 days with MC3T3-E1 cells in the extracts of as-extruded Mg–Sr alloys and pure Mg. In general, the gene expressions are time dependent. After 7 days of incubation, the extract of Mg–1.5Sr induces the highest Runx2 expression followed by the Mg–1.0Sr, Mg–0.25Sr, pure Mg and Mg–2.5Sr groups in sequence. For genes Opn, Sp7 and Bmp2, although no statistically significant differences are found among the various groups, Mg–Sr alloys groups still show higher expression levels, especially for Mg–1.0Sr and Mg–1.5Sr groups, than that of pure Mg. After culturing for 10 days, the Runx2 expressions of Mg–1.0Sr, Mg–1.5Sr and Mg–2.5Sr are much higher than that of pure Mg. The highest expressions of genes Opn and Sp7 are induced by the extracts of Mg–1.0Sr and Mg–1.5Sr, respectively. There is no statistical difference in the Bmp2 expression among the various groups. Then on day 14, Mg–Sr alloys, especially Mg–1.0Sr and Mg–1.5Sr, yield higher Runx2, Sp7 and Bmp2 expressions compared to the pure Mg group even though no statistical difference can be found for gene Opn. Generally, the Runx2, Opn, Sp7 and Bmp2 expressions of all the Mg–Sr samples increase at first and then decrease gradually with Sr contents increase. Mg–1.0Sr and Mg–1.5Sr show the most significant up-regulation of osteogenesis-related gene expressions.

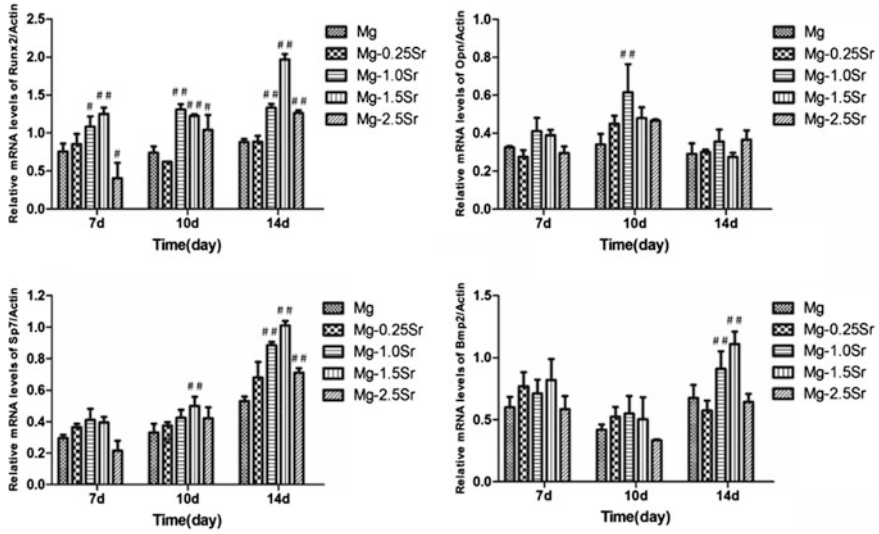


Fig. 8 Osteogenesis-related gene expressions by MC3T3-E1 cells after incubation for 7, 10 and 14 days in the extracts of as-extruded Mg–Sr alloys and pure Mg. #*p* < 0.05 and ##*p* < 0.01 compared to pure Mg

Conclusion

The present study systematically evaluates the cytocompatibility and osteogenic ability of the as-extruded Mg–xwt%Sr (*x* = 0.25, 1.0, 1.5, 2.5) alloys. No cytotoxicity towards MC3T3-E1 cells is observed for the Mg–Sr alloys and proper Sr alloying to Mg metal is favorable to enhance the adhesion, proliferation, alkaline phosphatase activity, matrix mineralization and collagen secretion of MC3T3-E1 cells. In particular, the optimal as-extruded Mg–1.5Sr alloy shows the best osteogenic differentiation inducibility. Our study suggests that degradable as-extruded Mg–Sr alloys with proper Sr content show good potential as orthopedic implants.

Acknowledgements This work was financially supported by the National Key Research on Development Program of China (No. 2016YFC1101804), National Natural Science Foundation of China (Nos.81401773, 51501218,81572113), the funding from Institute of Metal Research, Chinese Academy of Sciences (No.2015-ZD01), Guangdong Provincial Science and technology projects (2014A010105033), Guangdong Natural Science Foundation (2014A030310129), Shenzhen Peacock Programs (KQCX2014052111504544 and 110811003586331), Shenzhen-Hong Kong Technology Cooperation Funding Scheme (SGLH20150213143207910), Shenzhen Science and Technology Research Funding (JCYJ20160229195249481, JCYJ20160429185449249, JCYJ20160608153641 020) and the Public Technology Research Project of Zhejiang Province (Grant No.2016C31030).

References

1. F. Witte, J. Fischer, J. Nellesen, H.-A. Crostack, V. Kaese, A. Pisch, F. Beckmann, H. Windhagen, *Biomaterials* **27**, 1013–1018 (2006)
2. Y. Zhao, M.I. Jamesh, W.K. Li, G. Wu, C. Wang, Y. Zheng, K.W. Yeung, P.K. Chu, *Acta Biomater.* **10**, 544–556 (2014)
3. H. Yang, C. Liu, P. Wan, L. Tan, K. Yang, *APL Mater.* **1**, 052104 (2013)
4. D. Dziuba, A. Meyer-Lindenberg, J.M. Seitz, H. Waizy, N. Angrisani, J. Reifenrath, *Acta Biomater.* **9**, 8548–8560 (2012)
5. C. Liu, H. Yang, P. Wan, K. Wang, L. Tan, K. Yang, *Materials science & engineering. Mater. Biol. Appl.* **35**, 1–7 (2014)
6. L. Tan, X. Yu, P. Wan, K. Yang, *J. Mater. Sci. Technol.* **29**, 503–513 (2013)
7. C. Liu, X. Fu, H. Pan, W. Peng, W. Lei, L. Tan, K. Wang, Z. Ying, Y. Ke, P.K. Chu, *Sci. Rep.* **6**, 27374–27390 (2016)
8. D. Mantovani, H. Hermawan, D. Dube, *Acta Biomater.* **6**, 1693–1697 (2010)
9. S.K. Guan, H.X. Wang, X. Wang, C.X. Ren, L.G. Wang, *Acta Biomater.* **6**, 1743–1748 (2010)
10. M.P. Staiger, A.M. Pietak, J. Huadmai, G. Dias, *Biomaterials* **27**, 1728–1734 (2006)
11. L. Xu, E. Zhang, D. Yin, S. Zeng, K. Yang, *J. Mater. Sci. Mater. Med.* **19**, 1017–1025 (2008)
12. M. Bornapour, N. Muja, D. Shum-Tim, M. Cerruti, M. Pekguleryuz, *Acta Biomater.* **9**, 5319–5330 (2013)
13. X.N. Gu, X.H. Xie, N. Li, Y.F. Zheng, L. Qin, *Acta Biomater.* **8**, 2360–2374 (2012)
14. X.N. Zhang, J.N. Li, Y. Song, S.X. Zhang, C.L. Zhao, F. Zhang, L. Cao, Q.M. Fan, T.T. Tang, *Biomaterials* **31**, 5782–5788 (2010)
15. L. Xu, G. Yu, E. Zhang, F. Pan, K. Yang, *J. Biomed. Mater. Res. Part A* **83**, 703–711 (2007)
16. Y.F. Zheng, Z.J. Li, X.N. Gu, S.Q. Lou, *Biomaterials* **29**, 1329–1344 (2008)
17. N. Hort, Y. Huang, D. Fechner, M. Stormer, C. Blawert, F. Witte, C. Vogt, H. Drucker, R. Willumeit, K.U. Kainer, F. Feyerabend, *Acta Biomater.* **6**, 1714–1725 (2010)
18. R. Walter, M.B. Kannan, *Mater. Lett.* **65**, 748–750 (2011)
19. S. El-Rahman, *Pharmacol. Res.* **47**, 189–194 (2003)
20. Y. Nakamura, Y. Tsumura, Y. Tonogai, T. Shibata, Y. Ito, *Toxicol. Sci.* **37**, 106–116 (1997)
21. X. Zeng, Y. Wang, W. Ding, A.A. Luo, K. Sachdev Anil, *Metall. Mater. Trans. A* **37A**, 1333–1341 (2006)
22. Y. Fan, G.H. Wu, C.Q. Zhai, *Mater. Sci. Forum* **5**, 567–570 (2007)
23. Y. Li, Q. Li, S. Zhu, E. Luo, J. Li, G. Feng, Y. Liao, J. Hu, *Biomaterials* **31**, 9006–9014 (2010)
24. P.J. Marie, *Osteoporos. Int. : J. Established Result Cooperation Between Eur. Foundation Osteoporos. Nat. Osteoporos. Foundation USA* **16**(Suppl 1), S7–10 (2005)
25. J.Y. Reginster, O. Bruyere, A. Sawicki, A. Roces-Varela, P. Fardellone, A. Roberts, J. P. Devogelaer, *Bone* **45**, 1059–1064 (2009)
26. R. Rizzoli, R.D. Chapurlat, J.M. Laroche, M.A. Krieg, T. Thomas, I. Frieling, S. Boutroy, A. Laib, O. Bock, D. Felsenberg, *Osteoporos. Int.: J. Established Result Cooperation Between Eur. Foundation Osteoporos. Nat. Osteoporos. Foundation USA* **23**, 305–315 (2012)
27. J. Yan, J.F. Sun, P.K. Chu, Y. Han, Y.M. Zhang, *J. Biomed. Mater. Res. Part A* **101**, 2465–2480 (2013)
28. G.X. Ni, Z.P. Yao, G.T. Huang, W.G. Liu, W.W. Lu, *J. Mater. Sci. Mater. Med.* **22**, 961–967 (2011)
29. H.S. Brar, J. Wong, M.V. Manuel, *J. Mech. Behav. Biomed. Mater.* **7**, 87–95 (2012)
30. C. Liu, P. Wan, L.L. Tan, K. Wang, K. Yang, *J. Orthop. Transl.* **2**, 139–148 (2014)